

## Influence of Synthesis Route on the Formaldehyde Gas Sensing Properties of Nickel Oxide Nanostructures

Driss Lahem<sup>1</sup>, Roussin Lontio Fomekong<sup>2,3</sup>, John Ngolui Lambi<sup>3</sup>,  
Arnaud Delcorte<sup>2</sup>, Laurent Bilteryst<sup>4</sup>, Maurice Gonon<sup>5</sup>, Marc Debliquy<sup>5</sup>

<sup>1</sup> Department of Materials Science, Materia Nova ASBL Mons, Belgium

<sup>2</sup> Institute of Condensed Matter and Nanosciences, Université catholique de Louvain, UCL, Louvain-La-Neuve, Belgium

<sup>3</sup> Chemistry Department, Higher Teacher Training College, University of Yaoundé I, Yaounde, Cameroon

<sup>4</sup> Certech, R&D Institute, Senefte, Belgium

<sup>5</sup> Service Science des Matériaux, Faculté Polytechnique de Mons, UMONS, Mons, Belgium

**ABSTRACT:** NiO nanostructures can be used as materials for semiconductor gas sensors to detect formaldehyde, an indoor pollutant gas, at low concentrations (< 1 ppm). In this paper, the effect of the morphology of the synthesized NiO nanostructures on gas sensing properties is reported and discussed. The NiO nanostructures were synthesized by thermal decomposition of precursors obtained by two different chemical precipitation methods, a hydrothermal route and a sol-gel technique. Thick films (8-10  $\mu\text{m}$ ) of the synthesized NiO nanostructures were deposited by spray coating on alumina substrates fitted with gold interdigitated electrodes and a platinum heater. The gas sensing properties of these NiO layers were studied for low concentrations of formaldehyde gas at different working temperatures. A clear difference in response characteristics was observed between the samples prepared by the different synthesis routes employed. These differences can be ascribed to the surface microstructure of materials.

**Keywords:** Chemical precipitation, formaldehyde sensor, hydrothermal, indoor pollution, nickel oxide, sol-gel

### I. INTRODUCTION

In Europe and the United States, formaldehyde is nowadays considered by the authorities as one of the priority pollutants in indoor air because of its carcinogenic character and because of the plurality of its sources in our closed environment: paper products, stiffeners, wrinkle resisters and water repellents, insulation, varnishes, combustion devices, pressed-wood products, etc. The WHO guideline for indoor air formaldehyde concentration is 80 ppb (0.1  $\text{mg}/\text{m}^3$ ) [1].

It, therefore, seems necessary to measure the concentration of formaldehyde in closed environments since this data is essential for preventive actions (choice of the materials/furniture treatment, ventilation or indoor air purification). Several chemical and biochemical sensors (indicator tubes, electrochemical cells...) have been subject of numerous studies [2-5]. However, these inexpensive and miniature sensors are lacking in selectivity and due to relatively high detection limits, may not be suitable for "indoor" monitoring with the useful range being typically 10 ppb to 1 ppm.

Among the available gas sensing methods, the semiconducting metal oxide gas sensor devices have several unique advantages such as low cost, small size, measurement simplicity, durability, ease of fabrication and low detection limits [6].

Indeed, for the detection of formaldehyde, HCHO, various metal oxides have been studied including particularly the n-type semiconducting oxides  $\text{SnO}_2$ ,  $\text{ZnO}$ ,  $\text{WO}_3$  and  $\text{In}_2\text{O}_3$  [7-11]. P-type metal oxide semiconductors have also been studied as sensing materials for HCHO detection [12,13]. As an important p-type semiconductor, nickel oxide (NiO) has been investigated due to its catalytic properties for the oxidation of formaldehyde [14-16].

However, one of the critical issues currently limiting the wide use of these oxides is their lack of selectivity towards formaldehyde [17].

To overcome the problem of cross-sensitivity and enhance the HCHO sensitivity, various ways have been suggested in the literature, which include the addition of a noble catalytic metal (such as platinum and gold) and the use of composite metal oxides. Indeed, various sensitive materials such as doped- $\text{SnO}_2$  [18-20],

doped-ZnO [21,22], doped-CuO [13], CdO-mixed  $\text{In}_2\text{O}_3$  [23],  $\text{LaFe}_{1-x}\text{Zn}_x\text{O}_3$  [24],  $\text{La}_{1-x}\text{Pb}_x\text{FeO}_3$  [17] and Cd-doped  $\text{TiO}_2\text{-SnO}_2$  [25] have been reported to be selective and more sensitive to HCHO at ppm levels.

Nickel oxide (NiO), as a p-type wide-band gap (3.6–4.0 eV) semiconductor metal oxide, is a very promising material. NiO-based nanostructures and thin films have been extensively applied as antiferromagnetic materials [26], electrochromic films for smart windows [27], electrodes for batteries [28] and fuel cells [29] and as catalysts [30]. As gas sensor, NiO films were investigated for  $\text{H}_2$ ,  $\text{CH}_4$ ,  $\text{NH}_3$  and high concentration formaldehyde detection (detection limits 40 ppm and 100 ppm) [14,31, 32]. NiO thin film has already been pointed out as a sensitive material for formaldehyde detection at low concentrations [12,15,33]. Because of its applications in various fields, many synthesis routes for NiO nanoparticles or films have been proposed [34].

In most applications, the quality and structure of the nanomaterials undoubtedly play a crucial role in determining their performance. With the rising interest in engineering the morphology of NiO nanomaterials during the past decade, it has been established that the performance of NiO nanomaterials is also deeply affected by its morphology characteristics [35-37].

Controlling the morphology of nickel oxide nanostructures is crucial to obtain excellent physical and chemical performances [38-39]. There are many techniques available to synthesize the NiO nanostructures with different morphologies. Among them are the hydrothermal route [40], reflux method [41], thermal decomposition [42], chemical precipitation [43], microwave-assisted route [44] and the electro-spinning method [45].

Dirksen et al have reported that the morphology and structural properties of NiO thin layer have an influence on HCHO detection [14]. In addition, in one of our previous works [16], we showed with some first results that the synthesis route for the NiO is of primary importance on HCHO sensing behaviours.

In this paper, we present the characteristics of thick layers of nickel oxide synthesized by three different methods (chemical precipitation, sol-gel and hydrothermal) from four precursors and compare their performances towards formaldehyde detection in the ppb range.

## II. EXPERIMENTAL METHODOLOGY

### 2.1 Synthesis of the Nickel Oxide powders

NiO powders were synthesized by three different methods: sol-gel from nickel chloride, precipitation methods from nickel malonate and nickel sulfate precursors and hydrothermal route from nickel nitrate.

#### 2.1.1 By Sol-gel method [46]

$\text{NiCl}_2 \cdot 6\text{H}_2\text{O}$  (1.5 g, 6.3 mmol) was dissolved in 70 ml of absolute ethanol at room temperature, leading to a clear green coloured solution. In another beaker, NaOH (0.5 g, 12.5 mmol) was dissolved in 100 ml absolute ethanol and the NaOH solution was added to the nickel chloride solution dropwise. The mixture was stirred at room temperature for 2 h. During this time, the reaction mixture was found to form light green coloured gel. After 2 h, the gel was filtered, washed thoroughly with distilled water and then finally with ethanol. The precipitate was air dried, yielding a light green powder. TGA data showed that this green powder decomposes at  $\sim 294^\circ\text{C}$ .

#### 2.1.2 By precipitation from nickel sulfate [46]

83 mmol (5 g) of urea was added to 5.2 mmol (1.37 g) of nickel sulphate dissolved in 80 ml of distilled water and the mixture heated at  $80^\circ\text{C}$  for 4 h. The green precipitate formed was filtered, washed with distilled water several times to remove the unreacted nickel salt and urea and finally with absolute ethanol, and dried at room temperature. TGA data showed that the green powder decomposes at  $\sim 369^\circ\text{C}$ .

#### 2.1.3 By precipitation from nickel malonate [47]

Here, the NiO was obtained via two experimental steps: the synthesis of the precursor by precipitation in aqueous solution containing nickel ions using the malonate ligand as precipitating agent and its subsequent decomposition. Using nickel malonate precursor, lithium malonate was first prepared in aqueous solution by adding lithium hydroxide (10 mmol) to malonic acid (5 mmol) and the pH adjusted to 7. After 5 min, an aqueous solution containing nickel chloride was poured drop by drop into the previously prepared solution of lithium malonate with continuous stirring. The resulting green solution was then stirred for 3h at  $90^\circ\text{C}$  under reflux. The precipitate obtained was filtered, washed successively with distilled water, isopropanol and acetone, to ensure the total removal of impurities, and dried in an oven at  $70\text{-}80^\circ\text{C}$  resulting into a light green powder. The as-prepared precursor powder was calcined in a ceramic crucible at  $500^\circ\text{C}$  in a muffle oven ( $10^\circ\text{C}/\text{min}$ ) for 1 h under airflow. The TGA data obtained showed that the green powder decomposes at  $\sim 343^\circ\text{C}$ .

### 2.1.4 By hydrothermal procedure from nickel nitrate [48]

0.7 g (2.4 mmol) of  $\text{Ni}(\text{NO}_3)_2 \cdot 6\text{H}_2\text{O}$  and 0.5 g PEG 6000 were dissolved completely under rigorous magnetic agitation in 45 mL of distilled water and 2.5 mL of triethylamine  $\text{N}(\text{C}_2\text{H}_5)_3$  added to the above system dropwise and the stirring continued for 50 min. Finally, the mixture was transferred into a stainless steel autoclave which was sealed and maintained at 140 °C for 12 h. After the autoclave was allowed to cool naturally to room temperature, the resulting green precursor was filtered, washed several times with distilled water and ethanol successively and dried in vacuum at 80 °C for 12 h. TGA data showed that the green powder decomposes at ~337 °C.

### 2.2 Sensor preparation and gas sensing measurements

For gas sensing measurements, the synthesized powders were subjected to calcination at 400 °C for 1 h and each coated on alumina substrates fitted with interdigitated gold electrodes and platinum heating element (Fig. 1a) by simple spray-coating of the corresponding ink. The ink was prepared by mixing the metal oxide powder with distilled water and the resulting solution (charged with 10 % of metal oxide) was placed for 24 h in a TURBULA Shaker-Mixer to separate all the agglomerate particles. The thickness of the sensitive layers is ~8-10 μm (checked with an optical profiler). Finally, the NiO coatings were annealed at 400 °C for 1 h in air before their exposure to the gases.

The sensors were exposed to HCHO in the ppb level in a Teflon chamber as shown in Fig. 1b. The concentration of HCHO was controlled using a flow mass controller and measured by a HCHO-Analyzer (Process Mass Spectrometer AirSense). The moist air was obtained by humidification of dry air through a water bubbler maintained at 22 °C as presented in Fig. 1b.

## III. RESULTS AND DISCUSSION

In order to obtain information about the surface morphology and particle size of the samples, an FE-SEM analysis was performed. Fig. 2 shows the FE-SEM images of four NiO layers synthesized via three different methods.

It can be seen that the NiO layer obtained by the sol-gel method is present two kinds of spherical particle (Fig. 2a). Small particles of about 30 nm and much larger particles (~100 nm) are visible (Fig. 2a). In the sample obtained by precipitation from nickel malonate (Fig. 2b), NiO is composed of agglomerates of fine particles. The sample synthesized from nickel nitrate precursor exhibits a geometrically sheet-like 2D structure (Fig. 2c) whereas in the case of the sulfate precursor (Fig. 2d), the particles possess an agglomerated hexagonal sheet-like morphology forming 3D spherical structures.

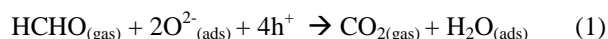
The XRD patterns of calcined samples were recorded by mean of a Bruker D5000 theta-theta diffractometer using  $\text{Cu } k\alpha_1$  radiation and a back monochromator and are shown in Fig. 3. The XRD patterns of powders prepared by precipitations from nickel malonate and nickel sulfate and by hydrothermal process from nickel nitrate (Figs. 3b, 3c and 3d, respectively) revealed the formation of face-centered-cubic NiO (JCPDS file N° 47-1049) [49]. The XRD pattern of the calcined sample prepared by sol-gel method from nickel chloride, however, showed additional peaks (Fig. 3a) which were identified as to the hexagonal nickel oxide  $\text{Ni}_2\text{O}_3$  (JCPDS file N° 14-0481) [49-51]. The presence of this oxide is certainly due to the transformation of a part of  $\text{Ni}(\text{OH})_2$  to  $\text{Ni}_2\text{O}_3$  enhanced in the presence of alkali metal cation  $\text{Na}^+$  [51,52].

Crystals sizes were determined using Scherrer relation from the FWHM of the (111), (200) and (220) diffraction peaks after subtraction of the  $k_{a2}$  and of the instrumental contribution to the broadening. The sizes obtained from the three peaks are close to each other, excepted for the sulfate powder (Table 1). For this later, we assume a strong anisotropy of the crystals shape.

We also determined the crystals size of phase  $\text{Ni}_2\text{O}_3$  from peaks (002), (200) and (202) (Fig. 3a). The  $\text{Ni}_2\text{O}_3$  crystals size obtained is about 130 nm. This could explain that the small particles observed for the sample prepared from chloride (Fig. 2a) correspond to NiO phase while larger particles correspond to the  $\text{Ni}_2\text{O}_3$  phase.

In order to compare the effect of the various NiO synthesis methods on the formaldehyde sensor response, electrical resistances of sensing layers were recorded with formaldehyde diluted in humid clean air (RH=50 %) at concentrations under 1 ppm at different operating temperatures (between 150 and 280 °C). The setup for the exposure tests of sensors to formaldehyde is shown in Fig. 1.

Since NiO is a p-type semiconductor, the electric resistance of NiO sensor increases when formaldehyde gas is introduced into the testing chamber. In fact, the HCHO molecules react with the adsorbed oxygen which leads to a reduction in the density of holes (eq.1) [12].



The sensor response, R, described in this paper is defined according to the eq. 2:

$$R = \frac{R_g - R_a}{R_a} \times 100 \quad (2)$$

Where  $R_a$  and  $R_g$  are the resistances of sensor in clean air and after exposure to formaldehyde, respectively.

Figs. 4 to 6 show the dynamic response of the various NiO-based sensors operated at 150, 200 and 250 °C. It can be seen from these figures that at higher temperatures, the NiO sample prepared by precipitation from malonate gives the best sensor response to formaldehyde (Fig. 6). At lower temperatures, however, the samples fabricated by the sol-gel method from nickel chloride and the hydrothermal process from nickel nitrate give a better response with good response times. On the other hand, the response of the NiO sample prepared by precipitation from nickel sulfate is very small and slow at working temperatures less than 250 °C. It can also be observed that for all temperatures, the response and recovery times of the sensors based on the nickel chloride route are shorter.

The sensing characteristics of these NiO-films to formaldehyde are, therefore, strongly influenced by the surface microstructure and the synthesis method.

The more favourable microstructure, in terms of sensitivity and response time, corresponds to that of the NiO sample obtained by the sol-gel method from nickel chloride. A possible reason for that is the morphology of the layers that show very fine particles in a highly porous stacking. The influence of the presence of  $Ni_2O_3$  phase cannot be excluded and must be investigated to better understand.

For this sensor, the effect of change in humidity of wet air from 10% RH to 80% RH is shown in Fig. 7. The results demonstrate that at working temperatures above 150 °C, NiO sensors have a good stability of operating parameters with respect to air humidity between 30% RH and 80% RH.

Studies have shown that alcohols and aromatic hydrocarbons are among the most important VOC compounds identified in indoor air [53].

That is why the different sensors were then studied with respect to several potential interfering gases belonging to these categories: ethanol, methanol, benzene and toluene. No response was observed at 5 ppm of toluene and benzene.

The results of ethanol and methanol tests are summarized in Table 2. Table 2 shows the response to 5 ppm of the gases for the different synthesis methods expressed in equivalent concentrations of formaldehyde (tests performed at the maximum sensitivity temperature, 200 °C).

This table shows that the chloride route leads to more selective sensors towards alcohols.

#### IV. CONCLUSIONS

NiO nanostructures were synthesized following different routes to compare the gas sensing performances of NiO coatings used as metal oxide sensors. The different synthesis routes led to various morphologies and this study demonstrated its strong influence on the gas sensing performance towards formaldehyde. The results showed that NiO is able to detect very low concentration of formaldehyde (<1 ppm) with good performance (good response, weak influence of humidity and good selectivity towards other VOC's). These results are promising for the development of simple and inexpensive devices allowing for monitoring in real time of formaldehyde in parts per billion (ppb) in indoor air.

#### ACKNOWLEDGEMENTS

This work was carried out in the framework of the CAPTINDOOR project of Materia Nova, UMONS and CERTECH, financially supported by the Walloon Region of Belgium. The authors also thank UCL for the scholarship program "Coopération au Développement". A. Delcorte is a Research Director of the Belgian National Science Foundation (FNRS).

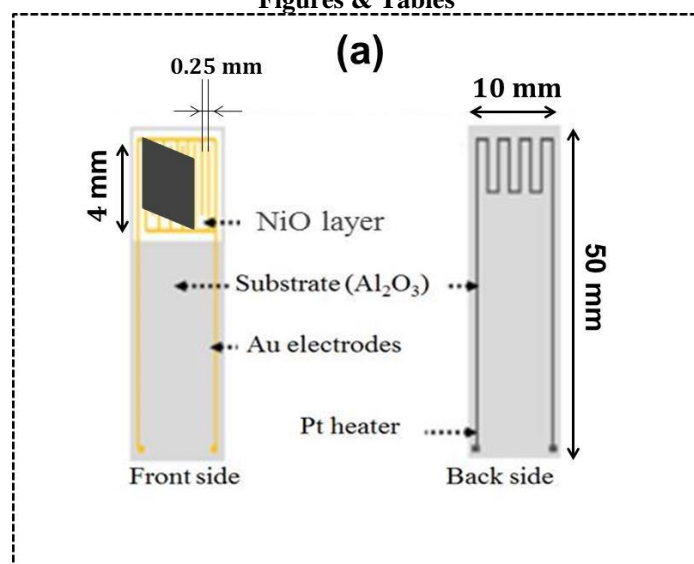
#### REFERENCES

- [1]. World Health Organization, Regional Office for Europe, WHO guidelines for indoor air quality: selected pollutants, Geneva 2010, ISBN: 9789289002134.
- [2]. P.-R. Chung, C.-T. Tzeng, M.-T. Ke, C.-Y. Lee, Formaldehyde Gas Sensors: A Review, *Sensors*, 13, 2013, 4468-4484.
- [3]. Á. González-Vila, M. Debliquy, D. Lahem, C. Zhang, P. Mégret, C. Caucheteur, "Molecularly imprinted electropolymerization on a metal-coated optical fiber for gas sensing applications, *Sens. Actuators B*, 244, 2017, 1145-1151.
- [4]. X. Tang, J.-P. Raskin, D. Lahem, A. Krumpmann, A. Decroly, M. Debliquy, A formaldehyde sensor based on molecularly imprinted polymer on  $TiO_2$  nanotube array, *Sensors*, 17, 2017, 1-15.
- [5]. Á. González-Vila, M. Debliquy, D. Lahem, P. Mégret, C. Caucheteur, Formaldehyde sensing with plasmonic near-infrared optical fiber grating sensors, *Proc. SPIE 9899, Optical Sensing and Detection IV*, 989917, 2016.

- [6]. S. M. Kanan, Oussama M. El-Kadri, I. A. Abu-Yousef, M. C. Kanan, Semiconducting Metal Oxide Based Sensors for Selective Gas Pollutant Detection, *Sensors*, 9, 2009, 8158-8196.
- [7]. L. Daza, S. Dassy, B. Delmon, Chemical sensors based on SnO<sub>2</sub> and WO<sub>3</sub> for the detection of formaldehyde: cooperative effects, *Sens. Actuators B*, 10, 1993, 99-105.
- [8]. D.-S. Lee, J.-K. Jung, J.-W. Lim, J.-S. Huh, D.-D. Lee, Recognition of volatile organic compounds using SnO<sub>2</sub> sensor array and pattern recognition analysis, *Sens. Actuators B*, 77, 2001, 228-236.
- [9]. B.L. Zhu, C.S. Xie, W.Y. Wang, Improvement in gas sensitivity of ZnO thick film to volatile organic compounds (VOCs) by adding TiO<sub>2</sub>, *Mater. Lett.*, 58, 2004, 624-629.
- [10]. A.K. Srivastava, Detection of volatile organic compounds (VOCs) using SnO<sub>2</sub> gas-sensor array and artificial neural network, *Sens. Actuators B*, 96, 2003, 24-37.
- [11]. X. Lai, D. Wang, N. Han, J. Du, J. Li, C. Xing, Y. Chen, X. Li, Ordered Arrays of Bead-Chain-like In<sub>2</sub>O<sub>3</sub> Nanorods and Their Enhanced Sensing Performance for Formaldehyde, *Chem. Mater.*, 22, 2010, 3033-3042.
- [12]. I. Castro-Hurtado, J. Herrán, G.G. Mandayo, E. Castaño, Studies of influence of structural properties and thickness of NiO thin films on formaldehyde detection, *Thin Solid Films*, 520, 2011, 947-952.
- [13]. X. Gou, G. Wang, J. Yang, J. Park, D. Wexlera, Chemical synthesis, characterisation and gas sensing performance of copper oxide nanoribbons, *J. Mater. Chem.*, 18, 2008, 965-969.
- [14]. J. A. Dirksen, K. Duval, T. A. Ring, NiO thin-film formaldehyde gas sensor, *Sens. Actuators B*, 80, 2001, 106-115.
- [15]. C.Y. Lee, C.M. Chiang, Y.H. Wang, R.H. Ma, A self-heating gas sensor with integrated NiO thin-film for formaldehyde detection, *Sens. Actuators B*, 122, 2007, 503-510.
- [16]. Lahem D, Lontio F.R et al, Formaldehyde gas sensor based on nanostructured nickel oxide and the microstructure effects on its response, *Proceedings IC-MAST2015 IOP Conf. Series: Materials Science and Engineering*, 2016, 108.
- [17]. L. Zhang, J.F. Hu, P. Song, H. Qin, X. Liu, M. Jiang, Formaldehyde sensing characteristics of perovskite La<sub>0.68</sub>Pb<sub>0.32</sub>FeO<sub>3</sub> nano-materials, *Physica B*, 370, 2005, 259-263.
- [18]. J. Wang, L. Liu, S.Y. Cong, J.-Q. Qia, B.-K. Xub, An enrichment method to detect low concentration formaldehyde, *Sens. Actuators B*, 134, 2008, 1010-1015.
- [19]. J. Wang, P. Zhang, J.-Q. Qi, P.-J. Yao, Silicon-based micro-gas sensors for detecting formaldehyde, *Sens. Actuators B*, 136, 2009, 399-404.
- [20]. P. Lv, Z.A.Tang, J. Yu, F. T. Zhang, G. F. Wei, Z. X. Huang, Y. Hu, Study on a microgas sensor with SnO<sub>2</sub>-NiO sensitive film for indoor formaldehyde detection, *Sens. Actuators B*, 132, 2008, 74-80.
- [21]. N. Han, Y. Tian, X. Wu, Y. Chen, Improving humidity selectivity in formaldehyde gas sensing by a two-sensor array made of Ga-doped ZnO, *Sens. Actuators B*, 138, 2009, 228-235.
- [22]. N. Han, L. Chai, Q. Wang, Y. Tian, P. Deng, Y. Chen, "Evaluating the doping effect of Fe, Ti and Sn on gas sensing property of ZnO", *Sens. Actuators B*, 147, 2010, 525-530.
- [23]. Chen T, Zhou Z, Wang Y, "Effects of calcining temperature on the phase structure and the formaldehyde gas sensing properties of CdO-mixed In<sub>2</sub>O<sub>3</sub>", *Sens. Actuators B*, 135, 2008, 219-223.
- [24]. S. Huang, H. Qin, P. Song, M. Jiang, The formaldehyde sensitivity of LaFe<sub>1-x</sub>Zn<sub>x</sub>O<sub>3</sub>-based gas sensor *J. Mater. Sci.*, 42, 2007, 9973-9977.
- [25]. W. Zeng, T. Liu, Z. Wang, S. Tsukimoto, M. Saito, Y. Ikuhara, Selective Detection of Formaldehyde Gas Using a Cd-Doped TiO<sub>2</sub>-SnO<sub>2</sub> Sensor, *Sensors*, 9, 2009, 9029-9038.
- [26]. X. L. Wang, P. S. Ku, Q. Shao, W. F. Cheng, C. W. Leung, A. Ruotolo, "Magnetism as a probe of the origin of memristive switching in p-type antiferromagnetic NiO" *Appl. Phys. Lett.*, 103, 2013, 223508.
- [27]. G. Bodurov, P. Stefchev, T. Ivanova, K. Gesheva, Investigation of electrodeposited NiO films as electrochromic material for counter electrodes in "Smart Windows", *Materials Letters*, 117, 2014, 270-272.
- [28]. M. Y. Cheng, Y. S. Ye, T. M. Chiu, C. J. Pan, B. J. Hwang, "Size effect of nickel oxide for lithium ion battery anode, *J. Power Sources*, 253, 2014, 27-34.
- [29]. N. Shaigan, D.G. Ivey, W. Chen, Electrodeposition of Ni/LaCrO<sub>3</sub> Composite Coatings for Solid Oxide Fuel Cell Stainless Steel Interconnect Applications, *J. Electrochem. Soc.*, 155, 2008, D278-D284.
- [30]. Q. Dong, S. Yin, C. S. Guo, X. Y. Wu, N. Kumada, T. Takei, A. Miura, Y. Yonesaki, T. Sato, Single-crystalline porous NiO nanosheets prepared from β-Ni(OH)<sub>2</sub> nanosheets: Magnetic property and photocatalytic activity, *Appl. Catal. B Environ.*, 147, 2014, 741-747.
- [31]. A. M. Soleimanpour, A. H. Jayatissa, G. Sumanasekera, Surface and gas sensing properties of nanocrystalline nickel oxide thin films, *Applied Surface Science*, 276, 2013, 291-297.
- [32]. S. Shijiu, Z. Kailiang, W. Fang, Y. Yujie, H. Yemei, Z. Tiantian, W. Meng, L. Chunjing, Gas Sensing Properties of Formaldehyde Sensor Based on Zn-, Cu-Doped NiO Thin Film, *ECS Transactions*, 60, 2014, 1115-1120.
- [33]. U. Cindemir, Z. Topalian, L. Österlund, C. G. Granqvist, G. A. Niklasson, "Porous Nickel Oxide Film Sensor for Formaldehyde", *J. Phys.: Conf. Ser.* 559 (2014) 1-5.
- [34]. Y. Wu, Y. He, T. Wu, T. Chen, W. Weng, H. Wan, Influence of some parameters on the synthesis of nanosized NiO material by modified sol-gel method, *Materials Letters*, 61, 2007, 3174-3178.
- [35]. Y. Q. Zhang, X. H. Xia, J. P. Tu, Y. J. Mai, S. J. Shi, X. L. Wang, C. D. Gu, Self-assembled synthesis of hierarchically porous NiO film and its application for electrochemical capacitors, *J. Power Sources*, 199, 2012, 413-417.
- [36]. J. Wang, H. Pang, J. Yin, L. Guan, Q. Lu, F. Gao, Controlled fabrication and property studies of nickel hydroxide and nickel oxide nanostructures", *Cryst. Eng. Comm.*, 12, 2010, 1404-1409.

- [37]. H. Liu, X. N. Dong, C. Y. Duan, X. Su, Z. F. Zhu, Three-dimensional hierarchical nickel-based hydroxides and oxides microspheres and their electrochemical properties, *Micro Nano Lett.*, 8, 2013, 745-748.
- [38]. L. Chu, M. Li, Z. Wan, L. Ding, D. Song, S. Dou, J.i Chen, Y. Wang, Morphology control and fabrication of multi-shelled NiO spheres by tuning the pH value via a hydrothermal process, *Cryst. Eng. Comm.*, 16, 2014, 11096-11101.
- [39]. F. Iqbal Dar, K. R. Moonosawmy, M. Es-Souni, Morphology and property control of NiO nanostructures for supercapacitor applications, *Nanoscale Research Letters*, 8, 2013, 1-7.
- [40]. D. Wang, P. Yang, Q. Ma, Y. Cao, A. Zhang, B. Huang, Micro- and nano-structures of iron oxide with tunable morphologies fabricated via solvothermal process, *Cryst. Eng. Comm.*, 15, 2013, 8959-8965.
- [41]. M. Liu, J. Chang, J. Sun, L. Gao, Synthesis of porous NiO using NaBH<sub>4</sub> dissolved in ethylene glycol as precipitant for high-performance supercapacitor, *Electrochim. Acta*, 107, 2013, 9-15.
- [42]. X. Wang, L. Wan, T. Yu, Y. Zhou, J. Guan, Z. Yu, Z. Li, Z. Zou, Non-basic solution eco-routes to nano-scale NiO with different shapes: Synthesis and application, *Mater. Chem. Phys.*, 126, 2011, 494-499.
- [43]. B. Cheng, Y. Le, W. Q. Cai, J. G. Yu, Synthesis of hierarchical Ni(OH)<sub>2</sub> and NiO nanosheets and their adsorption kinetics and isotherms to Congo red in water, *J. Hazard. Mater.*, 185, 2011, 889-897.
- [44]. D. Mohammadyani, S.A. Hosseini, S.K. Sadmezhaad, NiO Nanoparticles Synthesis by Chemical Precipitation and Effect of Applied Surfactant on Distribution of Particle Size, *International Journal of Modern Physics: Conference Series* 5, 2012, 270-276.
- [45]. C. Pan, R. Ding, Y. Hu, G. Yang, Electrospinning fabrication of rime-like NiO nanowires/nanofibers hierarchical architectures and their photocatalytic properties, *Physica E*, 54, 2013, 138-143.
- [46]. P. Jeevanandam, V.R.R. Pulimi, Synthesis of nanocrystalline NiO by sol-gel and homogeneous precipitation methods, *Indian Journal Chemistry*, 51A, 2012, 586-590.
- [47]. R. Lontio Fomekong, P. Kenfack Tsobnang, D. Magnin, S. Hermans, A. Delcorte, J. Lambi Ngolui, Coprecipitation of nickel zinc malonate: A facile and reproducible synthesis route for Ni<sub>1-x</sub>Zn<sub>x</sub>O nanoparticles and Ni<sub>1-x</sub>Zn<sub>x</sub>O/ZnO nanocomposites via pyrolysis, *J. Solid State Chem.*, 230, 2015, 381-389.
- [48]. L. Pan, Shanshan Ma, L. Li, Y. Chen, Synthesis of Ag/NiO composite nanosheets and empty microspheres and their highly effective electrocatalytic properties, *J. Sol-Gel Sci. Technol.*, 72, 2014, 161-170.
- [49]. S. Han, H.-Y. Chen, C.-C. Chen, T.-N. Yuan, H. C. Shih, Characterization of Ni nanowires after annealing, *Materials Letters*, 61, 2007, 1105-1108.
- [50]. Y. Zhang, The first observation of Ni and Ni<sub>2</sub>O<sub>3</sub> phases in the sol-gel Ag-doped NiO film, *Synthesis and Reactivity in Inorganic, Metal-Organic, and Nano-Metal Chemistry*, 46, 2016, 1565-1570.
- [51]. N. Srivastava, P.C. Srivastava, Realizing NiO nanocrystals from a simple chemical method, *Bull. Mater. Sci.* 33, 2010, 653-656.
- [52]. M. A. Aia, F. P. Kober, Methods for determining the structural and stoichiometric changes of Ni(OH)<sub>2</sub> electrodes during polarization in alkaline electrolyte, *American Chemical Society*, 11, 1967, 224-229.
- [53]. E. Gallego, X. Roca, J. F. Perales, X. Guardino, Determining indoor air quality and identifying the origin of odour episodes in indoor environments, *Journal of Environmental Sciences*, 21, 2009, 333-339.

**Figures & Tables**



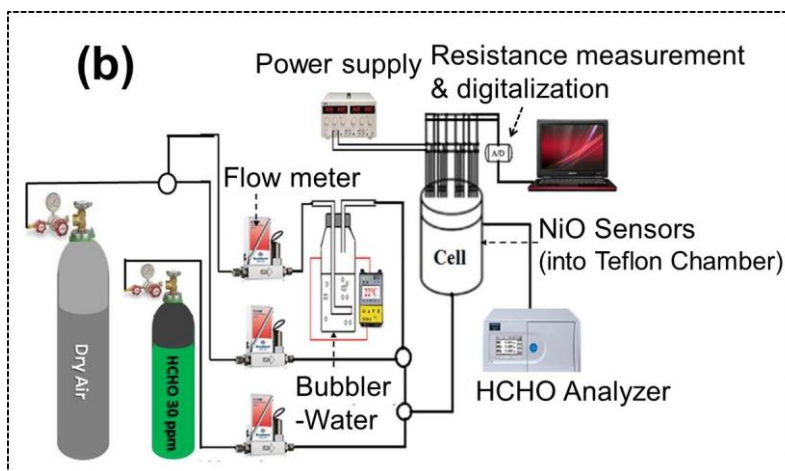


**Figure 1:** Substrate used for sensing measurement (a) and the setup used for formaldehyde sensing measurements (b).

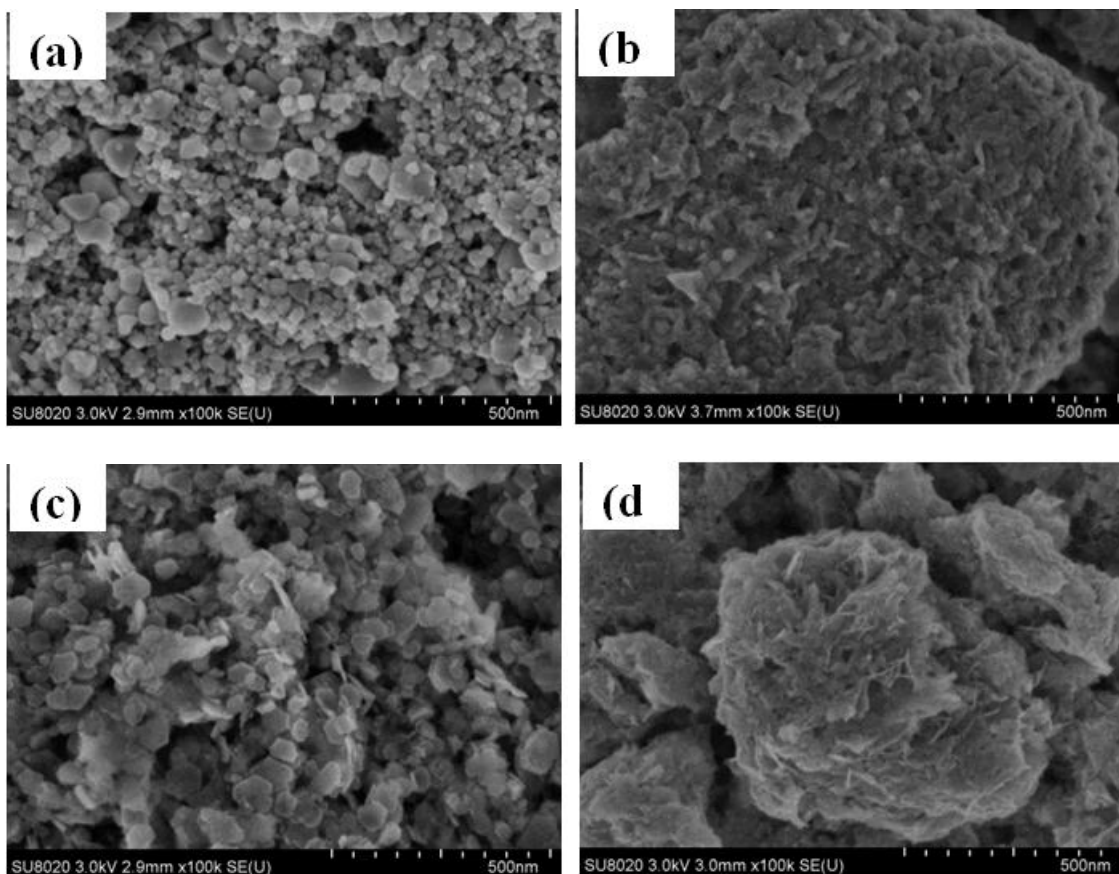


**Figure 2:** FE-SEM images of layers of NiO obtained from precursors prepared by (a) sol-gel from nickel chloride, (b) precipitation from nickel malonate, (c) hydrothermal route from nickel nitrate and (d) precipitation from nickel sulfate.

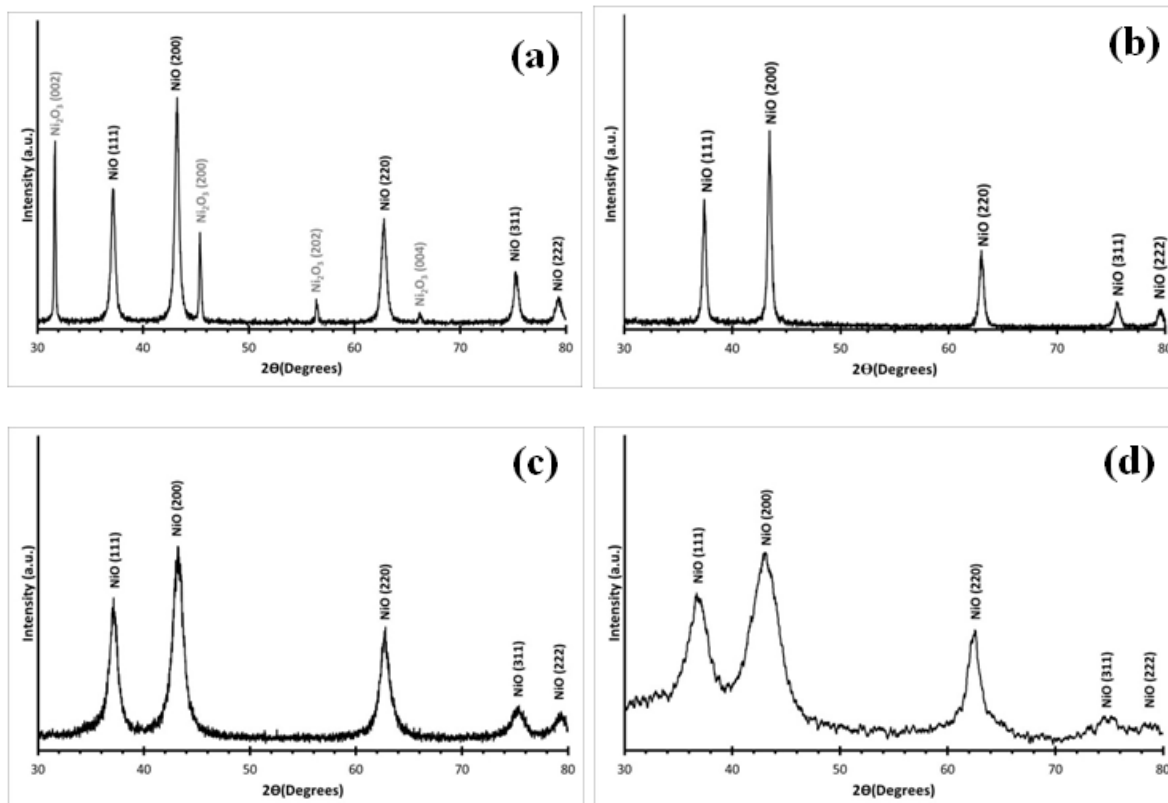


**Figure 3:** XRD patterns of NiO nanoparticles synthesized by sol-gel method from nickel chloride (a), by precipitation from nickel malonate (b), by hydrothermal process from nickel nitrate (c) and precipitation from nickel sulfate (d).

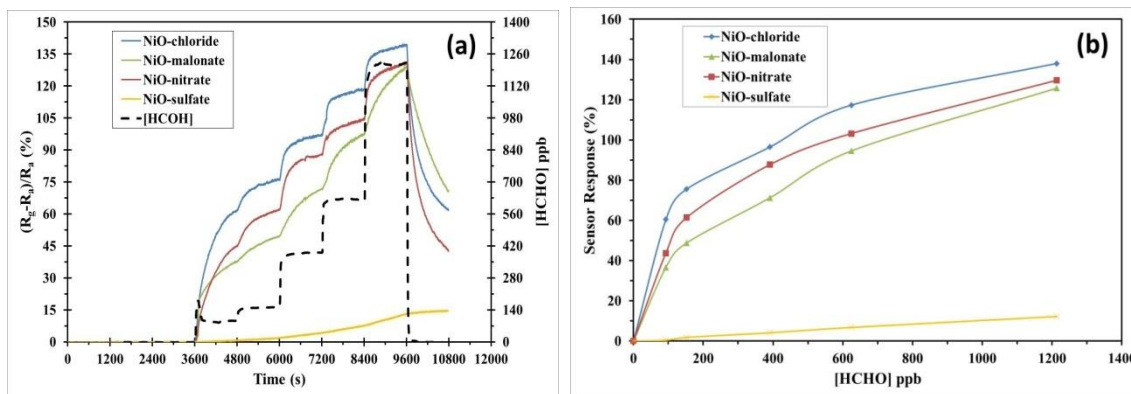


**Figure 4:** Dynamic response (a) and sensor response (b) of various NiO exposed to different concentrations of formaldehyde at T=150 °C.

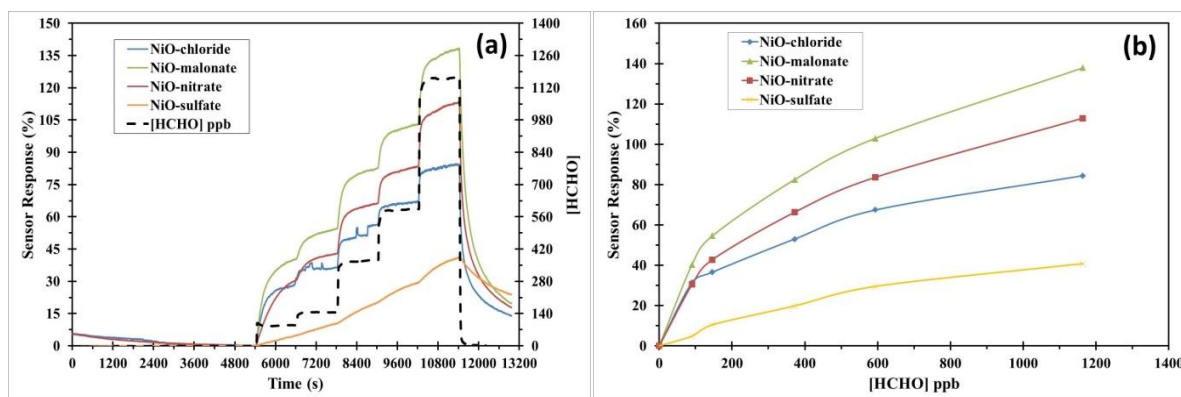


**Figure 5:** Dynamic response (a) and sensor response (b) of various NiO samples exposed to different concentrations of formaldehyde at T=200 °C.

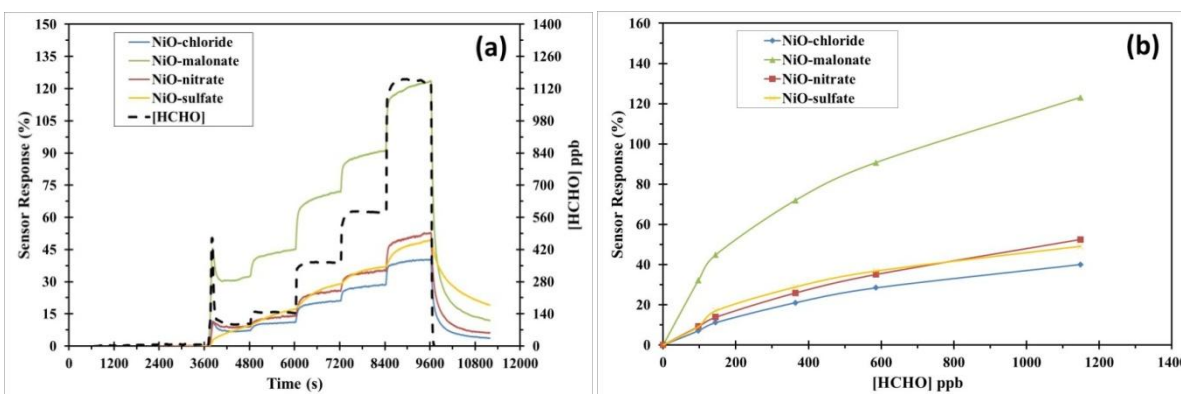


**Figure 6:** Dynamic response (a) and sensor response (b) of various NiO exposed to different concentrations of formaldehyde at T=250 °C.

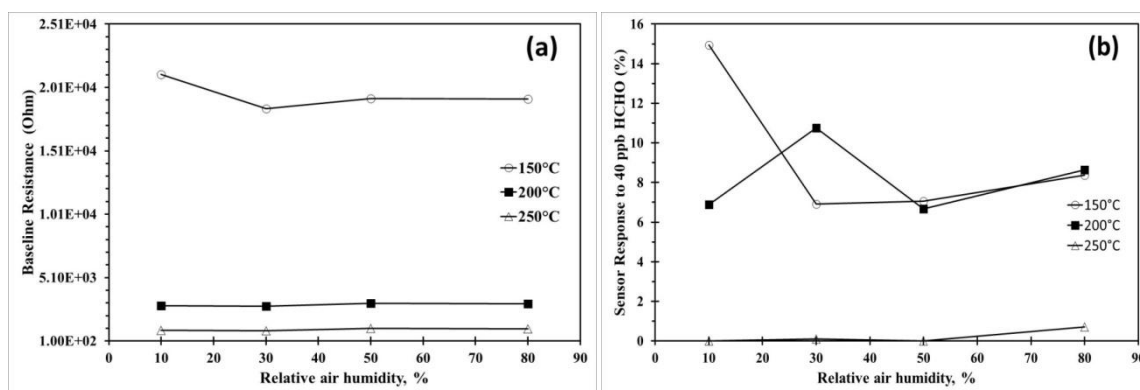


**Figure 7:** Influence of air humidity on baseline resistance (a) and on sensor response to 40 ppb (b) of sensor based on NiO from nickel chloride.

**Table 1:** Crystals sizes data of different NiO and Ni<sub>2</sub>O<sub>3</sub> samples collected by XRD of powders.

		Diffraction angle	Measured	Instrument	Sample	Crystal
Sample	Lattice plans	2-Theta °	FWHM	FWHM	FWHM	size
		2-Theta °	2-Theta °	2-Theta °	2-Theta °	nm
NiO-Chloride	(111)	37.10	0.308	0.131	0.281	33
NiO-Chloride	(200)	43.13	0.313	0.132	0.280	34
NiO-Chloride	(220)	62.69	0.391	0.135	0.366	28

Ni <sub>2</sub> O <sub>3</sub> -Chloride	(002)	31.62	0.149	0.130	0.072	126
Ni <sub>2</sub> O <sub>3</sub> -Chloride	(200)	45.36	0.155	0.132	0.081	118
Ni <sub>2</sub> O <sub>3</sub> -Chloride	(202)	56.36	0.147	0.134	0.060	165
NiO-Malonate	(111)	37.16	0.310	0.131	0.281	33
NiO-Malonate	(200)	43.21	0.262	0.132	0.226	42
NiO-Malonate	(220)	62.77	0.282	0.135	0.247	41
NiO-Nitrate	(111)	37.16	0.941	0.131	0.931	10
NiO-Nitrate	(200)	43.24	1.192	0.132	1.183	8
NiO-Nitrate	(220)	62.73	1.101	0.135	1.092	9
NiO-Sulfate	(111)	36.71	2.873	0.131	2.867	3
NiO-Sulfate	(200)	42.96	3.069	0.132	3.067	3
NiO-Sulfate	(220)	62.27	1.270	0.135	1.263	8

**Table 2:** Interference by methanol and ethanol.

	NiO-chloride (ppb)	NiO-nitrate (ppb)	NiO-malonate (ppb)
<b>Methanol 5 ppm</b>	95	130	310
<b>Ethanol 5 ppm</b>	80	105	470